Upwelling dynamics in the Baltic Sea studied by a combined SAR/infrared satellite data and circulation model analysis*

doi:10.5697/oc.55-3.687
OCEANOLOGIA, 55 (3), 2013.
pp. 687–707.

KEYWORDS
Baltic Sea
Coastal upwelling
MODIS and SAR images
Circulation model

Evgenia Gurova[1,⋆]
Andreas Lehmann[2]
Andrei Ivanov[3]

[1] Atlantic Branch of the P. P. Shirshov Institute of Oceanology of the Russian Academy of Sciences (IO RAS), Pr. Mira 1, 236000 Kaliningrad, Russia;

e-mail: evguruna@gmail.com

⋆corresponding author

[2] GEOMAR Helmholtz Centre for Ocean Research, Kiel, Germany;

e-mail: alehmann@geomar.de

[3] P. P. Shirshov Institute of Oceanology Moscow, Russia;

e-mail: ivanoff@ocean.ru

Received 21 February 2013, revised 6 May 2013, accepted 11 June 2013.

* The Envisat ASAR images used in this study were provided by ESA within the framework of the Envisat AO project C1P.3424, and C1P.8116. This work was supported by 1) the Russian Foundation for Basic Research, grant 12-05-90807-mol_rf_nr, and 2) the Russian Government (grant No. 11.G34.31.0078) for research under the supervision of leading scientists at the Russian State Hydrometeorological University.

Abstract

Data from the space-borne synthetic aperture radar (SAR) aboard the Envisat satellite and MODIS spectroradiometers on board the Terra/Aqua satellites, and the high resolution Sea Ice-Ocean Model of the Baltic Sea (BSIOM) have been used to investigate two upwelling events in the SE Baltic Sea. The combined analysis was applied to the upwelling events in July 2006 along the coasts of the Baltic States, and in June 2008 along the Polish coast and Hel Peninsula. Comparisons indicated good agreement between the sea surface temperatures and roughness signatures detected in satellite imagery and model results. It is shown that BSIOM can simulate upwelling events realistically. The utilization of modelled hydrodynamics and wind stress data together with SAR and SST information provides an extended analysis and deeper understanding of the upwelling processes in the Baltic Sea.

During the active phase of upwelling when the wind is strong, the resulting coastal jet is controlled by vorticity dynamics related to depth variations in the direction of the flow. Typical upwelling patterns are related to the meandering coastal jet and thus associated with topographic features. The longshore transport of the coastal jet is of the order of 10^4 m s^{-1}, and the offshore transport at the surface is of the order of 10^3 m s^{-1}, which respectively correspond to the total and largest river runoff to the Baltic Sea.

1. Introduction

Up- and downwelling are typical phenomena of the Baltic Sea (Lehmann & Myrberg 2008). Because of the Baltic's complex coastline and many islands, wind from any direction can in principal cause up- and downwelling off its coasts. The extent of upwelling is scaled by the internal Rossby radius, which for the Baltic is about 2–10 km. During summer and autumn, when the sea surface is warm, upwelling can be observed by infrared satellite measurements as a local temperature drop. Cold water from below the thermocline rises, eventually reaching the surface, where it replaces a well-mixed and considerably warmer upper layer. Generally, for upwelling to occur strong wind impulses are necessary. Typical time scales of upwelling range from a few days to weeks. Upwelling can be divided into two phases: 1) the active phase, when the wind is strong and cold water reaches the surface, and 2) the relaxation phase, when the wind has abated, but a strong temperature/density gradient persists. During the second phase filaments, squirts and whirls are often formed, most likely as a result of baroclinic instabilities in the coastal upwelling jet (Zhurbas et al. 2008). Satellite data indicate that the horizontal scales of coastal upwelling are of the order of 100 km alongshore and some 10–20 km offshore. Upwelled water sometimes spreads several tens of kilometres out into the open sea, forming filaments of cold water (e.g. Zhurbas et al. 2008, Laanemets et al. 2011).

Cold, upwelled water can bring about significant changes in the stability of the marine atmospheric boundary layer (MABL) as well as in the surface water density relative to surrounding waters. The lower wind stress caused by enhanced stability over colder and denser water leads to lower sea roughness, thereby creating areas of lower signal values in synthetic aperture radar (SAR) imagery. In other cases upwelling appears on SAR images as an area of alternate dark and light bands quasi-perpendicular to the coastline, not overlapping with sea surface temperature (SST) contours at all. The appearance of upwelling on SAR and SST images can have a varied correlation because of other factors affecting SAR imaging. High surface concentrations of floating cyanobacteria during summer blooms also give rise to changes in sea surface roughness (SSR) and can affect SAR imaging of upwelling (Gurova & Ivanov 2011). Such areas of cyanobacteria accumulations can be detected by the use of optical remote sensing data like MODIS under cloud-free conditions. Coastal upwelling along the Chinese coast in the Yellow Sea has been studied using multi-satellite sensors by Li et al. (2009). Those authors found a strong correlation between the low backscatter patterns in SAR with upwelling regions. However, upwelling is often an intermittent process, so that lowering in SST is not sustained. Furthermore, the strength and extent of upwelling signatures depends on the prehistory of upwelling events. When a chain of upwelling events is taking place, previous upwelling plays a part in the initial stratification for the next upwelling event; as a result a smaller wind impulse can impose the same upwelling strength in terms of SST decrease (Myrberg et al. 2010). On the other hand, related biogenetic slicks can cover the sea surface for a longer period if the wind conditions are suitable. Lin et al. (2002) found a correlation between radar backscatter and Chl *a* concentrations. From SAR images near-surface wind fields can be derived by using the CMOD4 wind scatterometer model (Stoffelen & Anderson 1997) for converting radar backscatter values into wind speeds and by taking the wind direction from atmospheric models or by inferring the direction from linear features visible on the SAR image. Recently, Gurova & Ivanov (2011) and Kozlov et al. (2011) presented studies of SAR imaging of coastal upwelling in the Baltic Sea. They demonstrated that the dark features visible on the SAR images in the coastal zones of the south-eastern Baltic Sea can be attributed to coastal upwelling events. Over upwelling areas the wind stress was significantly reduced if the mean wind speed was below a certain threshold (Kozlov et al. 2011).

To further investigate upwelling events detected in SAR/MODIS satellite images, a high resolution coupled Sea Ice-Ocean Model of the Baltic Sea (BSIOM) was applied. This model can simulate upwelling events

realistically (Lehmann et al. 2012). In a combined SAR/IR satellite and circulation model analysis we investigated specific coastal upwelling events in the Baltic Sea. The upwelling signature can be obtained from satellite images, and, additionally, the associated upwelling dynamics can be derived from the numerical model. This approach proved to be suitable for enhancing our knowledge of upwelling in the Baltic Sea.

The structure of the paper is as follows. In section 2, the material and methods used are described in some detail to explain the relation between the upwelling signatures detected in satellite images and model data. Then, the results of the combined analysis of two upwelling events occurring in July 2006 along the coasts of the Baltic States and in June 2008 along the Polish coast close to the Hel Peninsula (Figure 1) are presented in section 3. Finally, the discussion and conclusions are given in sections 4 and 5 respectively.

2. Material and methods

In our analysis we used Envisat ASAR images and MODIS Aqua/Terra SST data, as well as the high resolution coupled sea ice-ocean model (BSIOM), developed by GEOMAR (Kiel, Germany).

MODIS (Terra and Aqua) data (Table 1) at Level 1A were downloaded from the open-access NASA archive (http://ladsweb.nascom.nasa.gov/data/) and processed to Level 2 products using Seadas 6.2 (Update 2) software. The MUMM algorithm of atmospheric correction (Ruddick et al. 2000) was used, which allowed high-resolution processing to be performed at 500 m using the resolution of bands 3–7; it has to be borne in mind however, that the original sensor resolution for MODIS SST bands is 1 km. SST products were calculated using the standard algorithm implemented in Seadas 6.2 (Brown & Minnett 1999).

Wide Swath Mode (WSM) images from the C-band Advanced Synthetic Aperture Radar (ASAR) on board the Envisat satellite with a spatial resolution of 150 m (pixel size 75 m) were obtained from the ESA archives (Table 1). SAR measures the backscattered radar power or the normalized radar cross section (NRCS), which is a function of radar parameters, incidence angles, wind speed and direction (Valenzuela 1978). In fact, an SAR image is a 2D-picture of distribution of sea surface roughness acquired by spaceborne imaging radars. Many oceanic and atmospheric phenomena taking place in the upper ocean and the lower atmosphere leave characteristic footprints on SAR images in favourable wind conditions (Clemente-Colón & Yan 2000).

The numerical model used in this study is a general three-dimensional coupled sea ice-ocean model of the Baltic Sea (Lehmann & Hinrichsen 2000,

Table 1. Acquisition parameters of MODIS and ASAR images

Date	MODIS		ASAR (Envisat)	Wind (MODIS/ASAR)
	satellite	time, UTC	time, UTC	[m s^{-1}]
15.06.2006	Terra	09:20	–	14
16.07.2006	Aqua	11:50	20:05	11/5
19.07.2006	Aqua	10:45	20:11	4/0.3
28.05.2008	Aqua	11.35	–	5
29.05.2008	–	–	09:14	6
1.06.2008	Terra	10:15	–	5
2.06.2008	Aqua	11:10	20:13	2/3
3.06.2008	Terra	10:05	–	7
4.06.2008	Aqua	11:00	–	8
5.06.2008	Terra	09:55	–	5
6.06.2008	Terra	10:35	–	5
7.06.2008	Terra	09:40	–	3
8.06.2008	Terra	10:25	–	5

Lehmann et al. 2002). The horizontal resolution of the coupled sea-ice ocean model is at present 2.5 km, and in the vertical 60 levels are specified, which enables the upper 100 m to be resolved into levels of 3 m thickness. The model domain includes the Baltic Sea with the Kattegat and Skagerrak. At the western boundary, a simplified North Sea basin is connected to the Skagerrak to supply characteristic North Sea water masses in terms of temperature and salinity profiles resulting from the different forcing conditions (Lehmann 1995). Prescribed low frequency sea level variations in the North Sea/Skagerrak were calculated from the BSI (Baltic Sea Index, Lehmann et al. 2002, Novotny et al. 2006). The coupled sea ice-ocean model is forced by realistic atmospheric conditions taken from the Swedish Meteorological and Hydrological Institute (SMHI, Sweden) meteorological database (L. Meuller, pers. comm.), which covers the whole Baltic drainage basin on a regular grid of $1^\circ \times 1^\circ$ with a temporal increment of 3 hours. The database consists of synoptic measurements interpolated on the regular grid by using a 2D univariate optimum interpolation scheme. This database, which for modelling purposes is further interpolated onto the model grid, includes the surface pressure, precipitation, cloudiness, air temperature and water vapour mixing ratio at 2 m height and geostrophic wind. Wind speed and direction at 10 m height are calculated from geostrophic winds with respect to different degrees of roughness on the open sea and off the coast (Bumke et al. 1998). Forcing functions of BSIOM, such as wind stress, radiation and heat fluxes, were calculated according to Rudolph & Lehmann (2006). Additionally, river runoff was prescribed from a monthly mean runoff data set (Kronsell & Andersson 2012).

During the thermal-stratified period of the year, coastal upwelling can be detected as a decrease in sea surface temperature. Under cloud-free conditions, thermal IR-sensors such as the NOAA Advanced Very High Resolution Radiometer (AVHRR) are most commonly used to map areas of active upwelling. Lehmann et al. (2012) determined upwelling frequencies from satellite derived SST maps of the Baltic Sea and corresponding hydrodynamic model data. In the case of SAR, three key mechanisms are proposed to explain the lower radar returns observed in upwelling conditions: an increase in the atmospheric marine boundary layer stability, an increase in the viscosity of surface waters, and the presence of biogenic surfactants in the upwelling region (Mitnik & Lobanov 1991, Hsu et al. 1995, Clemente-Colón & Yan 1999).

The transformation of the atmospheric boundary layer over the upwelling area and the reduction of the sea surface roughness (SSR) due to lower sea surface temperatures decrease the wind stress. However, the reduction of SSR may also be due to upwelling-related biogenic slicks, which cause damping of capillary and short gravity waves. The interpretation of SAR imagery is complicated by other atmospheric and oceanic factors, so-called look-alikes, such as low wind speed, rain, or the presence of mineral and biogenic oily surfactants that result in low radar backscatter features (Clemente-Colón & Yan 2000).

The BSIOM wind stress calculation incorporates a natural way of replicating the changes in sea surface properties caused by variations in the air-sea temperature difference. The drag coefficient calculated according to Large & Pond (1981) depends on the roughness length and the stability correction. The roughness length z_0 is obtained by combining the aerodynamic roughness length z_c and the roughness length of a smooth surface z_s (Smith 1988),

$$z_0 = z_c + z_s = 0.0185u_*^2/g + 0.11v/u_*, \tag{1}$$

where the acceleration due to gravity $g = 9.8$ m s^{-2}, the kinematic viscosity of air $v = 14 \times 10^{-6}$ m^2 s^{-1} and the friction velocity is defined as

$$u_* = (\tau/\rho)^{1/2}, \tag{2}$$

where τ is the wind stress and ρ the density of air. The drag coefficient in neutral stratification is defined as

$$C_{\mathrm{DN}} = [K/\ln(z/z_0)], \tag{3}$$

where $K = 0.4$ is the von Karman constant. At wind speeds >5 m s^{-1}, z_c is dominant while z_s causes C_{DN} to increase at wind speeds <3 m s^{-1} (Smith 1988). The roughness length z_0 describes the surface due to the

state of the turbulence; it may be a complicated function of sea surface parameters (Large & Pond 1981). The momentum flux prescribed in BSIOM is described by the wind stress

$$\tau = \rho C_{\mathrm{D}} U^2 \tag{4}$$

and the drag coefficient is calculated according to Large & Pond (1981)

$$C_{\mathrm{D}} = K^2[\ln(z/z_0)\psi(z/L)]^{-2} \tag{5}$$

where $\psi(z/L)$ provides a stability correction. L is the stratification parameter, the Monin-Obukhov length. Thus, the wind stress will be reduced in upwelling areas where the stability increases. Hence, the calculated wind stress fields can be directly compared with SAR image signatures, so long as atmospheric forcing and the time of SAR acquisition agree, and BSIOM is able to produce upwelling with a similar temperature difference, and at the right location along the Baltic Sea coast.

Krauss & Brügge (1991) demonstrated that upwelling in the Baltic Sea should be regarded as a three-dimensional current system affecting not only the local coast but also the opposite coast and the interior of the basin (Fennel & Sturm 1992, Fennel & Seifert 1995). Krauss & Brügge (1991) described the principal response of a stratified elongated basin to constant wind along the basin. Assuming that the wind direction is parallel to the coast: (i) the wind impact results in Ekman transport perpendicular to the coastline in the surface layers; (ii) in the northern hemisphere this Ekman transport produces a local water level rise on the right-hand coast (as seen from the wind direction) and a fall on the left-hand side. Furthermore, downwelling occurs on the right-hand side and upwelling on the left-hand side, resulting in baroclinic effects of the same sign off both coasts; (iii) consequently coastal jets are produced along both coasts parallel to the wind direction, and a slow return flow compensates for this transport in the central area of the basin.

The coastal jet is related to the corresponding rise or fall in sea level close to the coast. Thus the flow is barotropic and geostrophically balanced. For barotropic geostrophic currents

$$U_g = -g/f\partial\eta/\partial y, V_g = g/f\partial\eta/\partial x. \tag{6}$$

On the assumption that the curl of the wind stress can be neglected, the vorticity production equation (see e.g. Csanady 1982) reduces to

$$\partial\zeta/\partial t = f/H\partial\eta/\partial t + f/HU_g\nabla H. \tag{7}$$

Thus, vorticity is generated through vortex stretching due solely to the rise and fall of the sea surface, and/or by depth variations, i.e. if the

geostrophic flow crosses depth contours (see Lehmann et al. (2002) for details).

3. Results

The July 2006 upwelling event

At the beginning of July 2006, weak winds prevailed over the eastern Gotland basin. During 14 July the wind speed increased to 10–12 m s^{-1}, the prevailing direction being from the north. On 15 July the wind speed reached its maximum of 15 m s^{-1}. These northerly winds decreased in speed until the night of 17 July 2006, when they backed to the west. On 18 July the direction returned to north, while the speed further decreased until 19

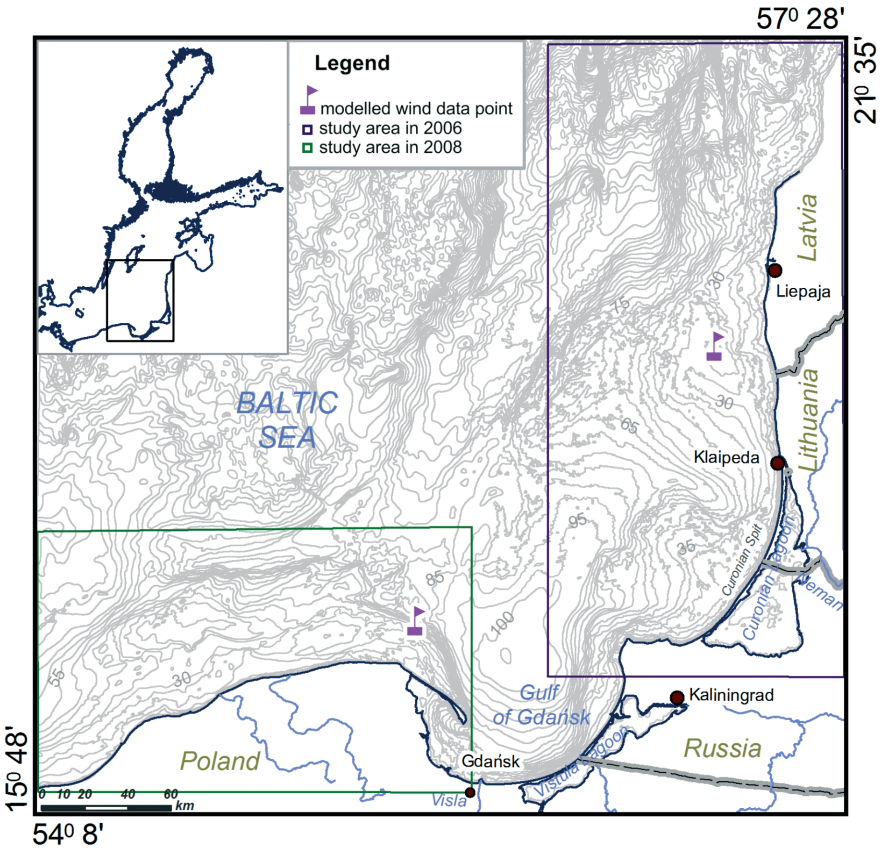

Figure 1. Map of the south-eastern Baltic Sea. The rectangles mark the study areas for upwelling in July 2006 and in May/June 2008. The purple symbols mark the positions where wind data were extracted from model wind forcing (bathymetry: Gelimbauskaite (1998))

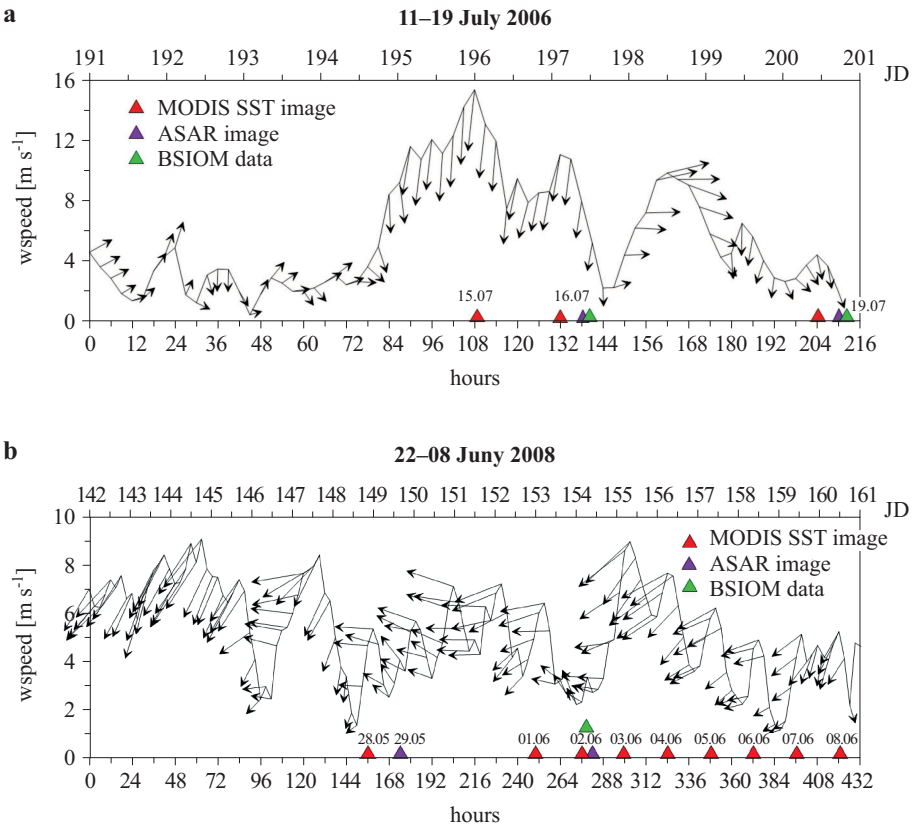

Figure 2. Wind speed and direction extracted at 10 m height in the areas of interest (Figure 1) at positions: a) 56°11.1′N, 20°36.6′E from 11–19 July 2006, and b) 55°09′N, 18°27′E from 22 May–8 June 2008. The dates and times of ASAR and MODIS image acquisitions are shown by coloured triangles

July (Figures 1 and 2). MODIS SST images were available for 15, 16 and 19 July and SAR images were taken on 16 and 19 July (Table 1, Figure 2). After one day of northerly winds, upwelling developed along the Latvian and Lithuanian coast, and on 16 July it developed further with specific patterns obviously related to topographic features (Figure 3a, b). The temperature gradient over the core of the upwelling to the open sea was about 10°C. Bychkova et al. (1988) observed similar features along this coast; according to Lehmann et al. (2012) the upwelling frequency is about 15% for July based on 88 weekly composite SST maps for the period 1990–2009.

The upwelling situation in July 2006 was also studied by Kozlov et al. (2011). Their analysis of SAR and MODIS images found that upwelling features were very distinct in SAR images. Here we extend this analysis by additionally utilizing a numerical model of the Baltic Sea. Figures

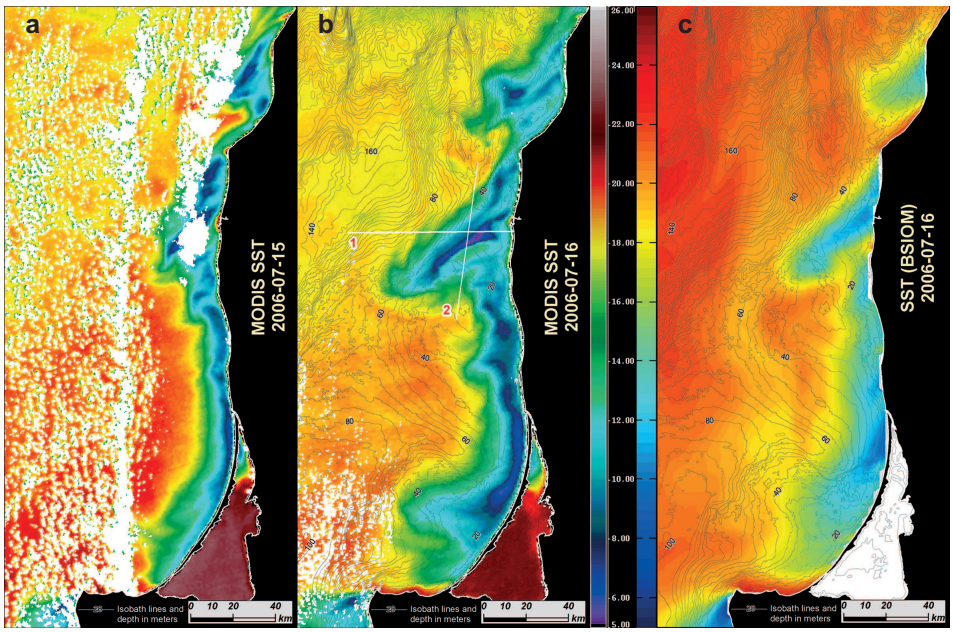

Figure 3. Sea surface temperature fields [°C] derived from MODIS data on 15 (a) and 16 July 2006 (b), and the BSIOM model on 16 July 2006 (c). For b) and c) the bottom topography is overlain. The lines on Figure (b) show the transects shown in Figure 5

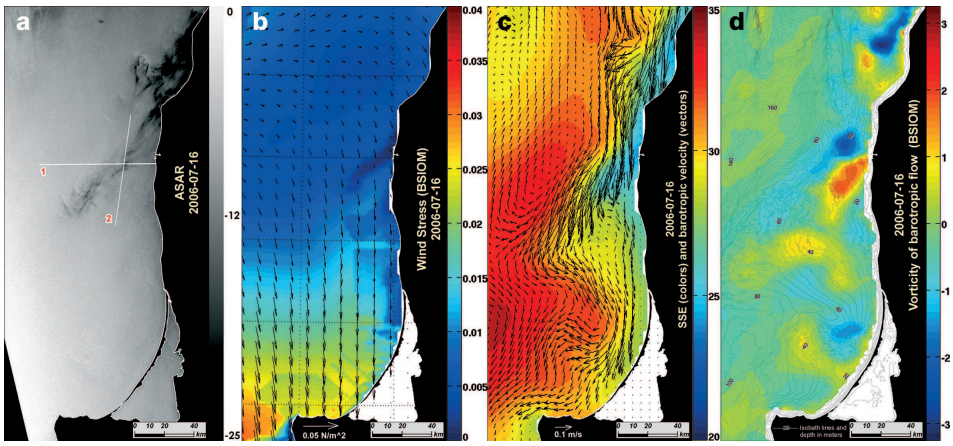

Figure 4. SAR image and modelling results for 16 July 2006: a) ASAR image, b) BSIOM wind stress [N m^{-2}], c) BSIOM sea surface heights [cm] and barotropic flow, d) BSIOM vorticity of the barotropic flow [s^{-1}]. The lines on Figure (a) show the transects shown in Figure 5

3c and 4 show simulated SST, sea level heights (SSH), the barotropic flow field and its relative vorticity on 16 July 2006. Owing to northerly winds, which triggered an Ekman transport offshore, there was a drop in SSH close to the coast and a corresponding, geostrophically balanced, coastal jet developed (Krauss & Brügge 1991). The location of the upwelling features are controlled by the interaction of the coastal jet and the bottom topography (Zhurbas et al. 2004). If the water depth decreases in the direction of the flow, negative relative vorticity is induced and the flow turns offshore; if the water depth increases, positive vorticity is induced and the flow turns back to the coast (Figure 4c,d). Thus, upwelling filaments in SST are related to the meandering coastal jet. Transports along and off the coast were calculated from the model. The transport of the coastal jet was

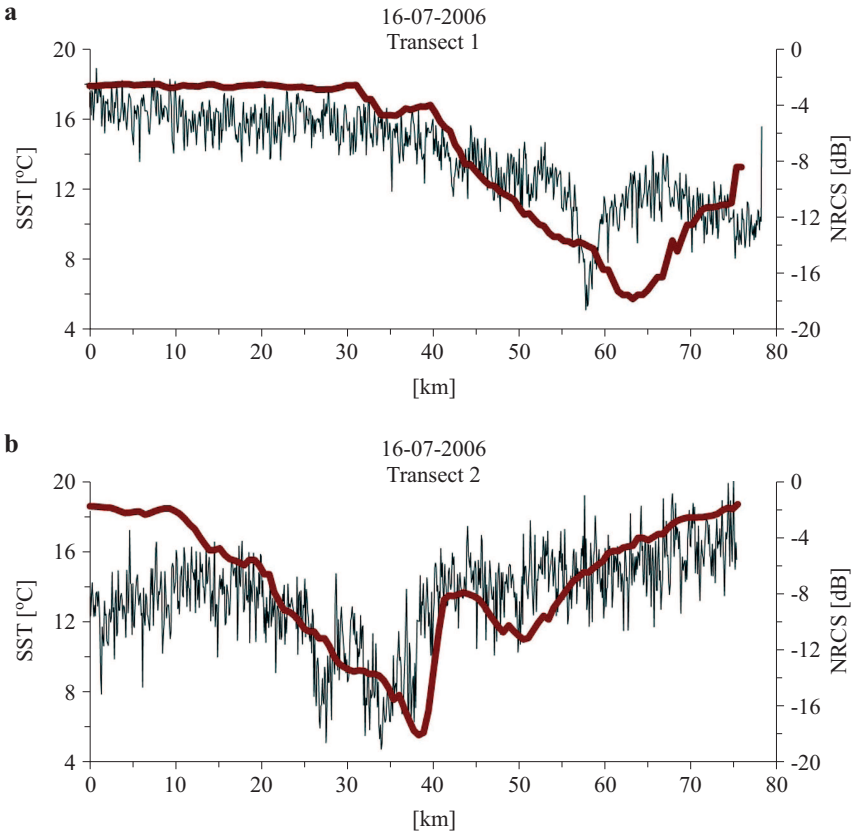

Figure 5. MODIS sea surface temperature [°C] (thick red line) and ASAR normalized radar cross section [dB] (black line) for 16 July 2006 along the transects 1 and 2 shown in Figure 3b. Note the different resolutions of 1 km and 150 m for the SST map and ASAR image respectively

as high as 4×10^3 m s^{-1} at the surface (average over the first 10 m), and 2.5×10^4 m s^{-1} over the whole water column. The offshore transport at the surface through a meridional section at 20.5°E was on average 4×10 m s^{-1}. The surface transport is thus comparable with the largest river runoff, and the total transport of the jet is even larger than the mean total runoff to the Baltic Sea, which is about 1.4×10^4 m s^{-1} (Kronsell & Andersson 2011).

The SAR image (Figure 4a) shows distinct structures of low backscatter correlated with the location of cold upwelled waters. However, the magnitude of the NCRS contrast is not uniform, becoming rather weak to the south (see also Kozlov et al. 2011). The reduced contrast is due to increasing surface winds (Figure 2a), which exert a higher wind stress and cause increasing roughness on the ocean surface (Figure 4b). The wind

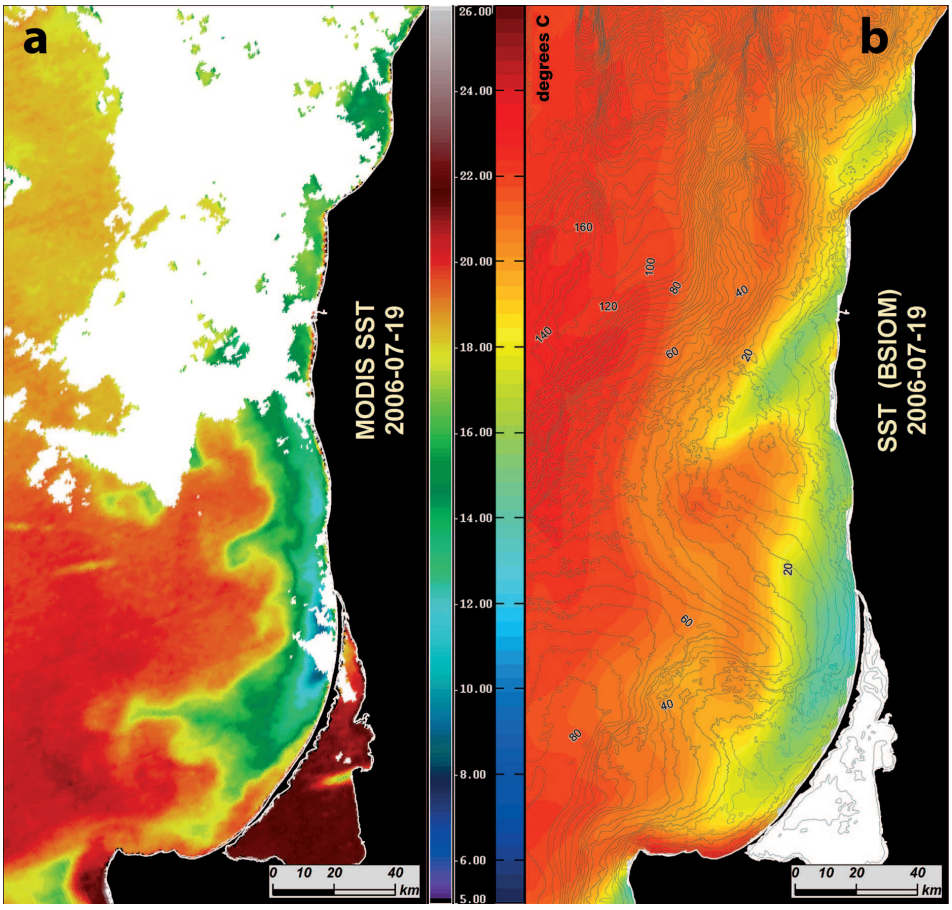

Figure 6. Sea surface temperature fields [°C] derived from MODIS data (a) and the BSIOM model (b) on 19 July 2006

stress reveals similar structures as the SAR image (Figure 4a,b). The areas of reduced backscatter coincide with the reduction in wind stress. Due to the cold upwelled water the stability increases and the wind stress is reduced according to equations (4) and (5).

Figure 5 shows latitudinal and meridional transects through the upwelling filament of 16 July 2006. There is a close coincidence between the SST and NRCS gradients. Note the different resolutions and time shift between the MODIS SST and ASAR images of 6 hours (Figure 2). It is clear that in these highly dynamic situations, the frontal area of the upwelling structure will probably be deformed because of baroclinic instabilities (Myrberg et al. 2010). However, the strong coincidence of the SAR backscatter and MODIS SST structures confirms that the signal in SAR images is due to changes in the MABL resulting from reduced SST (Lin et al. 2002, Li et al. 2009).

On 17 July 2006 the wind turned to the west increasing to 9 m s^{-1}, then turned back to north decreasing until 19 July to nearly windless conditions (Figure 2a). Consequently, the upwelling signal was much weaker compared to 16 July 2006 (compare Figures 3b–c and 6a–b). The cloudy area (Figure 6a) was associated with a southward movement of a weak front of higher wind speeds (Figure 7a), which was not resolved in the model forcing data (Figure 7b). However, the ASAR image and model wind stress show similar structures outside the cloud-covered area (Figure 7a, b). Because of the weak wind forcing, the Ekman drift at the surface was reduced, so there was only a slight drop in SSH towards the coast and the associated coastal jet was

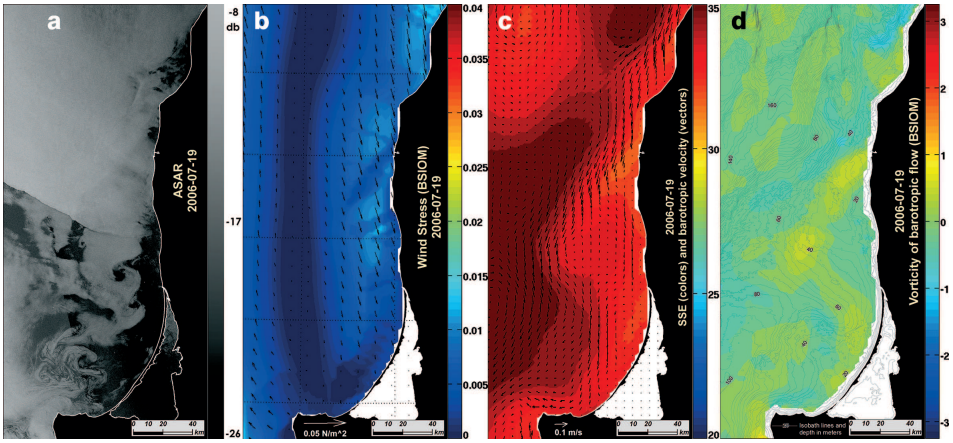

Figure 7. SAR image and modelling results for 19 July 2006: a) ASAR image, b) BSIOM wind stress [N m^{-2}], c) BSIOM sea surface heights [cm] and barotropic flow, d) BSIOM vorticity of the barotropic flow [s^{-1}]

very weak. Consequently, the vorticity structures were not as pronounced as on 16 July 2006 (compare Figures 4 and 7).

The June 2008 upwelling event

From the end of May to the beginning of June 2008 upwelling occurred along the Polish coast. Upwelling off the Hel Peninsula occurs with a frequency of 15–20% in May and June; this percentage is based on 89 and 86 weekly SST maps for the period 1990–2009 (Lehmann et al. 2012). This prominent upwelling event along the Polish coast has been analysed by several other authors (e.g. Zhurbas et al. 2004, Kowalewski & Ostrowski 2005, Myrberg et al. 2010). From 22 May to 7 June 2008 a period of easterly winds prevailed. However, from 22 to 25 May the wind was mostly onshore, turning to the east from 26 May to 7 June, and finally on 8 June turning to north – north-west with wind speed maxima fluctuating between 5 and 9 m s^{-1} (Figures 1 and 2). Easterly winds are the most likely to force upwelling along the coast of the Hel Peninsula and further to the west along the Polish coast. Again, upwelling structures were closely related to bottom topographic obstacles. The SST difference between upwelling and the unaffected area was about 6C. MODIS SST images were available on 28 May, 1 to 8 June (Figures 2 and 8), and ASAR images on 29 May and

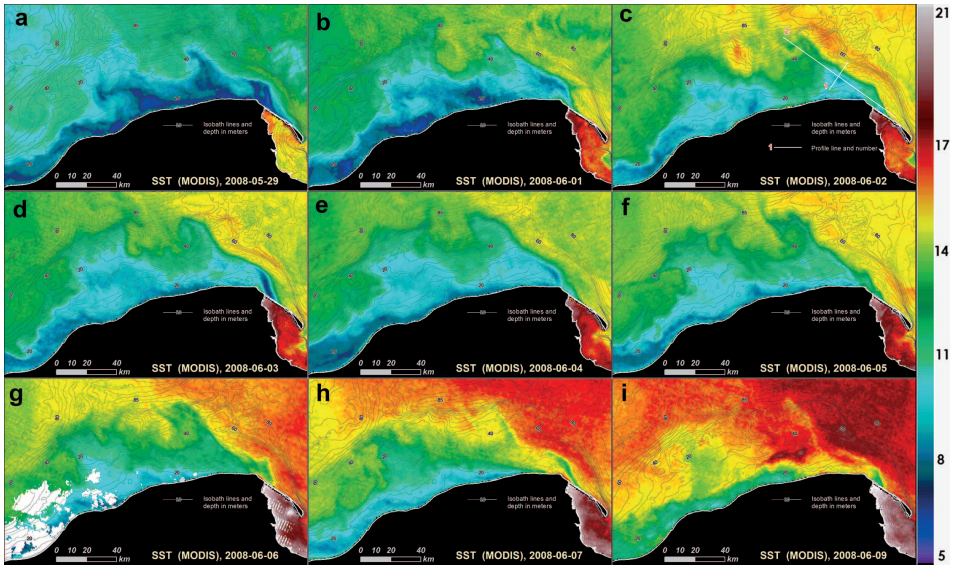

Figure 8. Development of upwelling along the Polish coast from 28 May to 8 June 2008 as seen in MODIS imagery (MODIS SSTs [°C] overlain with bottom topography)

2 June 2008 (Figures 2 and 9). The ASAR images show low backscatter north of the Hel Peninsula, which was even more pronounced on 2 June 2008. Again, similar structures, clearly related to the upwelling area, could

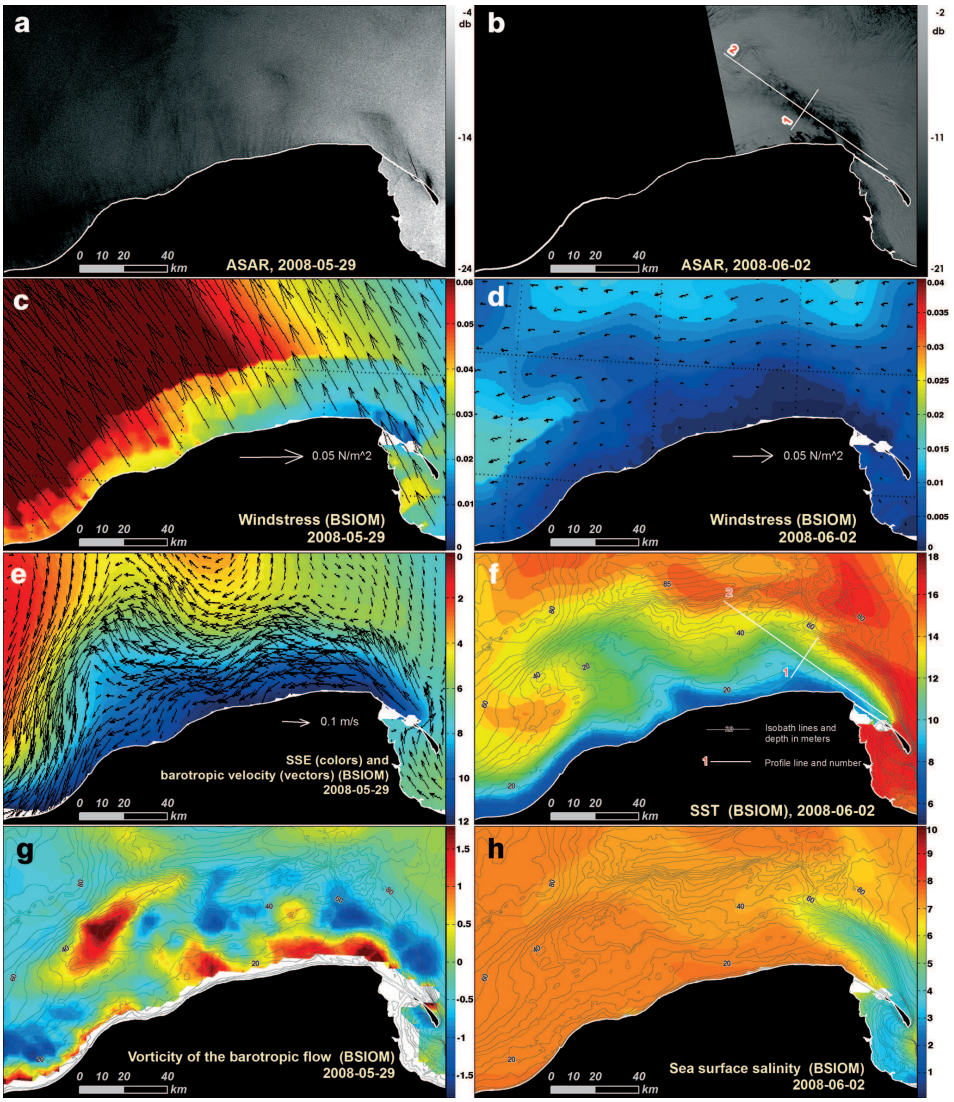

Figure 9. ASAR images and modelling results: a) ASAR image acquired on 29 May 2008, b) ASAR image acquired on 2 June 2008, c) BSIOM wind stress [N m^{-2}] on 29 May, d) BSIOM wind stress [N m^{-2}] on 2 June, e) BSIOM sea surface heights [cm] and barotropic flow on 29 May, f) BSIOM sea surface temperature [°C] on 2 May, g) BSIOM vorticity of barotropic flow [s^{-1}] on 29 May, h) BSIOM sea surface salinity [PSU] on 2 June 2008

be found in the wind stress fields (Figure 9). Compared with the situation in July 2006, the upwelling area was related to an associated drop in SSH and a coastal jet emerging at the tip of Hel Peninsula meandering further to the west. On 2 June 2008 the total transport of the jet was as high as 2×10^4 m^3 s^{-1}. The SST structures of the frontal area were related to the meandering jet controlled by the bottom topography (compare Figures 8 and 9e–f). Due to easterly winds, the Vistula river plume was pushed to the west of the Gulf of Gdańsk; on reaching the Hel Peninsula, it was then dragged westwards by the coastal jet, leading to a sharp frontal area between colder, more saline water and warmer, less saline water (Figure 9h). The coastal jet in this frontal area may easily become baroclinically unstable (Myrberg et al. 2010).

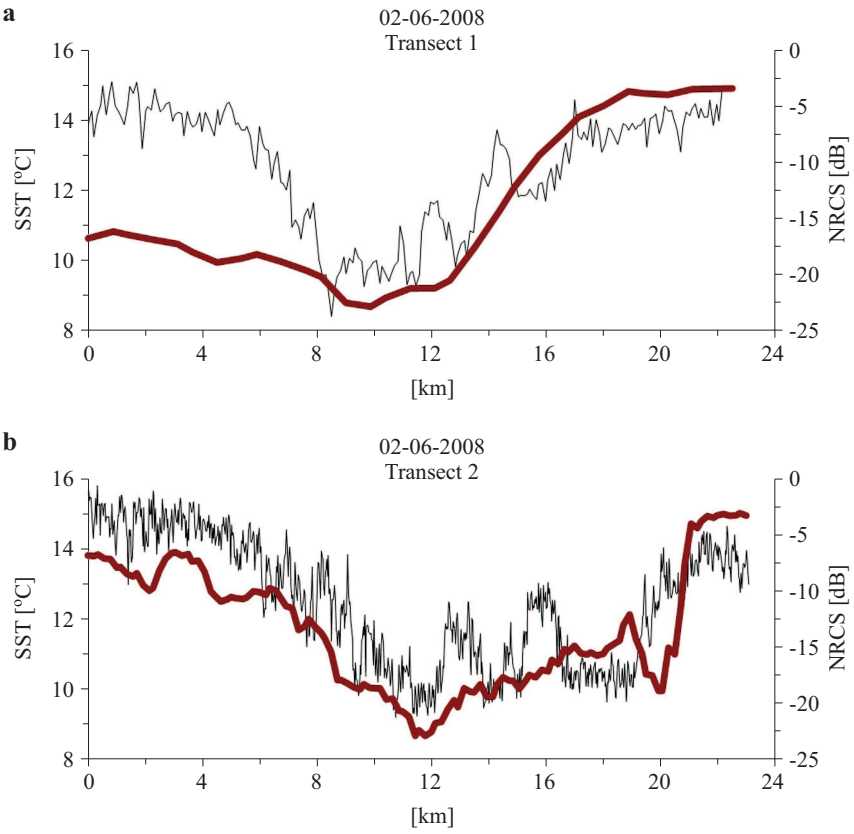

Figure 10. MODIS sea surface temperature [°C] (thick red line) and ASAR normalized radar cross section [dB] (black line) for 2 June 2008 along transects 1 and 2 shown on Figures 8c and 9b. Note the different resolutions of 1 km and 150 m for the SST map and ASAR image respectively

Transects through the upwelling frontal area on the ASAR and MODIS images of 2 June 2008 show very good agreement (Figure 10). Again, there was a slight shift of gradients, most probably because of frontal movement due to the time lapse between MODIS and ASAR data acquisition.

4. Discussion

It has been clearly demonstrated that a combined analysis of observations, in our case of remote sensing data and the results of numerical modelling, is superior to single methods alone in many ways. The utilization of modelled hydrodynamics and wind stress data together with SAR/IR information can provide an extended analysis and deeper understanding of the upwelling process in the Baltic Sea. The horizontal resolution of BSIOM seems to be appropriate for simulating upwelling in those regions of the Baltic Sea where the internal Rossby radius is between 5 and 10 km. To simulate the whole spectrum of mesoscale variability a horizontal resolution of at least 1 nautical mile is required (Zhurbas et al. 2008).

Infrared satellite images can be used to detect upwelling off the coast. Of course, cloud coverage is a problem, so that for most cases the whole upwelling event, normally lasting from several days up to weeks, cannot be observed completely by infrared satellite images. However, SAR can provide information on sea surface roughness even in cloud-covered situations. Increased stability of the MABL over cold upwelled water leads to lower sea surface roughness, creating areas of lower signal values in SAR imagery. However, SAR images are sensitive to changes in the background wind field. If a certain wind speed threshold, which depends on the across-front temperature gradient, is exceeded, the increase in sea surface roughness masks any structures of reduced backscatter related to cold upwelling (Kozlov et al. 2011), thus limiting the application of ASAR images to weak and moderate wind conditions. Furthermore, the appearance of upwelling on SAR images and SST maps can have a varied correlation because of other factors affecting SAR imaging. High surface concentrations of floating cyanobacteria during summer algae blooms also give rise to changes in sea surface roughness and can affect SAR imaging of upwelling. Such areas of cyanobacteria accumulations can be detected by the use of optical remote sensing data like MODIS under cloud-free conditions. Thus, the reduction of sea surface roughness in upwelling areas is due mainly to lower temperature and/or the presence of biogenetic films on the surface. For the analysis of upwelling it is necessary to discriminate between these two effects. A good indicator of these effects, mostly controlling the reduction in sea surface roughness, is the comparison of transects through the frontal region. If the

ASAR and SST gradients coincide, the reduction in SAR signal is most probably due to temperature reduction in upwelling areas.

It should be noted that BSIOM cannot simulate the occurrence of any surface slicks, so that the reduction in sea surface roughness (wind stress) is due solely to changes in the MABL. Furthermore, optical images, e.g. from the MODIS satellite, show that the concentration of total suspended matter in upwelling areas is reduced, and that the frontal areas coincide with the thermal front. Even chlorophyll concentrations are reduced, which is due to the fact that the upwelled water originates from deeper layers where the chlorophyll concentration is small. If the euphotic zone is depleted of nutrients, upwelling supplies nutrients from below the thermocline. This can eventually lead to phytoplankton blooming with a certain time lag. Upwelling in the Baltic Sea normally occurs within a few days; hence, the time is too short to trigger phytoplankton blooms that would change the nutrient content of the surface waters. In most cases, therefore, the reduction in SAR backscatter in coastal areas away from river mouths is due to changes in MABL over upwelling regions.

5. Conclusions

BSIOM can simulate the upwelling process reasonably well. Over upwelling areas where the SST is lowered, the wind stress (drag coefficient) is reduced if the wind speed is below a certain threshold (e.g. 5–7 m s^{-1}). Thus, SAR images and wind stress fields can show similar structures over upwelling areas. The greatest difficulty is to extract the model data exactly at the time when the SAR/MODIS images were taken; in other words the model needs to be forced by the most realistic atmospheric conditions.

According to Zhurbas et al. (2008), the upwelling process can be divided into two phases. The active phase is when the wind is strong, the inclination of the sea surface greatest and cold water reaches the surface. During this phase the coastal jet is mainly barotropic. This barotropic coastal jet is controlled by vorticity dynamics related to depth variations in the direction of the flow. Decreasing water depth leads to the jet being deflected from the coast, whereas increasing water depth causes it to return to the coast. The meandering of the coastal jet is associated with the position of upwelling structures. Thus, along the Baltic Sea coast, typical upwelling patterns will occur at the same locations during similar wind events. Transports related to the active phase of upwelling were found to be of the order of 10^3 m s^{-1} offshore at the surface, and 10^4 m s^{-1} alongshore associated with the meandering coastal jet.

In the relaxation phase, when the wind has weakened but a strong temperature/density gradient persists, the sea level inclination is reduced

and the flow field is determined mainly by the baroclinic coastal jet. During this phase the coastal jet may become baroclinically unstable, and filaments, squirts and whirls are often formed (Zhurbas et al. 2008).

References

Brown O. B., Minnett P. J., 1999, *MODIS infrared sea surface temperature algorithm theoretical basis document*, Ver. 2.0, (http://modis.gsfc.nasa.gov/data/atbd/atbd_mod25.pdf).

Bumke K., Karger U., Hasse L., Niekamp K., 1998, *Evaporation over the Baltic Sea as an example of a semi-enclosed sea*, Contr. Atmos. Phys., 71 (2), 249–261.

Bychkova I., Viktorov S., Shumakher D., 1988, *A relationship between the large-scale atmospheric circulation and the origin of coastal upwelling in the Baltic*, Metorol. Gidrol., 10, 91–98, (in Russian).

Clemente-Colón P., Yan X. H., 1999, *Observations of east coast upwelling conditions in synthetic aperture radar imagery*, IEEE T. Geosci. Remote, 37 (5), 2239–2248, http://dx.doi.org/10.1109/36.789620.

Clemente-Colón P., Yan X.-H., 2000, *Low backscatter features in SAR imagery*, JHU APL Tech. Digest, 21 (1), 116–121.

Csanady G. T., 1982, *Circulation in the coastal ocean*, D. Reidel Publ. Company, Dordrecht, 279 pp., http://dx.doi.org/10.1007/978-94-017-1041-1.

Fennel W., Seifert T., 1995, *Kelvin wave controlled upwelling in the western Baltic*, J. Marine Syst., 6 (4), 289–300, http://dx.doi.org/10.1016/0924-7963(94)00038-D.

Fennel W., Sturm M., 1992, *Dynamics of the western Baltic*, J. Marine Syst., 3 (1–2), 183–205, http://dx.doi.org/10.1016/0924-7963(92)90038-A.

Gelimbauskaite L.-Z. (ed.), 1998, *Bathymetric map of the Central Baltic Sea, scale 1:500 000*, LGT Ser. Marine Geol. Maps, No. 1 / SGU Ser. Ba No. 54., Geol. Survey Sweden, Lith. Inst. Geol., Vilnius/Uppsala.

Gurova E. S., Ivanov A. Yu., 2011, *Appearance of sea surface signatures and current features in the South-East Baltic Sea on the MODIS and SAR images*, Issled. Zemli Kosm., 4, 41–54, (in Russian).

Hsu M. K., Mitnik L. M., Liu C. T., 1995, *Upwelling area northeast of Taiwan on ERS-1 SAR images*, Acta Oceanogr. Taiwan., 34 (3), 27–38.

Kowalewski M., Ostrowski M., 2005, *Coastal up- and downwelling in the southern Baltic*, Oceanologia, 47 (4), 454–475.

Kozlov I. E., Kudryavtsev V. N., Johannessen J. A., Chapron B., Dailidiene I., Myasoedov A. G., 2011, *ASAR imaging for coastal upwelling in the Baltic Sea*, Adv. Space Res., 50 (8), 1125–1137, http://dx.doi.org/10.1016/j.asr.2011.08.017.

Krauss W., Brügge B., 1991, *Wind produced water exchange between the deep basins of the Baltic Sea*, J. Phys. Oceanogr., 21, 373–384, http://dx.doi.org/10.1175/1520-0485(1991)021<0373:WPWEBT>2.0.CO;2.

Kronsell J., Andersson P., 2012, *Total regional runoff to the Baltic Sea*, HELCOM Indicator Fact Sheets 2011, (http://www.helcom.fi/environment2/ifs).

Laanemets J., Váli G., Zhurbas V., Elken J., Lips I., Lips U., 2011, *Simulation of mesoscale structures and nutrient transport during summer upwelling events in the Gulf of Finland in 2006*, Boreal Environ. Res., 16 (Suppl. A), 15–26.

Large W. G., Pond S., 1981, *Open ocean flux measurements in moderate to strong winds*, J. Phys. Oceanogr., 11, 324–336, http://dx.doi.org/10.1175/1520-0485(1981)011<0324:OOMFMI>2.0.CO;2.

Lehmann A., 1995, *A three-dimensional baroclinic eddy-resolving model of the Baltic Sea*, Tellus A, 47 (5), 1013–1031, http://dx.doi.org/10.1034/j.1600-0870.1995.00206.x.

Lehmann A., Hinrichsen H.-H., 2000, *On the thermohaline variability of the Baltic Sea*, J. Marine Syst., 25, 333–357, http://dx.doi.org/10.1016/S0924-7963(00)00026-9.

Lehmann A., Krauss W., Hinrichsen H.-H., 2002, *Effects of remote and local atmospheric forcing on circulation and upwelling in the Baltic Sea*, Tellus A, 54 (3), 299–316.

Lehmann A., Myrberg K., 2008, *Upwelling in the Baltic Sea – A review*, J. Marine Syst., 74 (Suppl.), S3–S12, http://dx.doi.org/10.1016/j.jmarsys.2008.02.010.

Lehmann A., Myrberg K., Höflich K., 2012, *A statistical approach to coastal upwelling in the Baltic Sea based on the analysis of satellite data for 1990–2009*, Oceanologia, 54 (3), 369–393, http://dx.doi.org/10.5697/oc.54-3.369.

Li X. M., Li X. F., He M. X., 2009, *Coastal upwelling observed by multi-satellite sensors, Science in China*, Sci. China Ser. D, 52 (7), 1030–1038, http://dx.doi.org/10.1007/s11430-009-0088-x.

Lin I.-I., Wen L.-S., Liu K.-K., Tsai W.-T., Liu A.-K., 2002, *Evidence and quantification of the correlation between radar backscatter and ocean colour supported by simultaneously acquired in situ sea truth*, Geophys. Res. Lett., 29 (10), http://dx.doi.org/10.1029/2001GL014039.

Mitnik L. M., Lobanov V. B., 1991, *Reflection of the oceanic fronts on the satellite radar images*, [in:] *Oceanography of Asian marginal seas*, K. Takano (ed.), Elsevier Oceanogr. Ser., 54, Elsevier, Amsterdam, 85–101.

Myrberg K., Andrejev O., Lehmann A., 2010, *Dynamics of successive upwelling events in the Baltic Sea – a numerical case study*, Oceanologia, 52 (1), 77–99.

Novotny K., Liebsch G., Lehmann A., Dietrich R., 2006, *Variability of sea surface heights in the Baltic Sea: An intercomparison of observations and model simulations*, Mar. Geod., 29 (2), 113–134, http://dx.doi.org/10.1080/01490410600738054.

Ruddick K. G., Ovidio F., Rijkeboer M., 2000, *Atmospheric correction of SeaWiFS imagery for turbid coastal and inland waters*, Appl. Optics, 39 (6), 897–912.

Rudolph C., Lehmann A., 2006, *A model-measurements comparison of atmospheric forcing and surface fluxes of the Baltic Sea*, Oceanologia, 48 (3), 333–380.

Smith S. D., 1988, *Coefficients for the sea surface wind stress, heat flux, and wind profiles as a function of wind speed and temperature*, J. Geophys. Res., 93 (C12), 15467–15472, http://dx.doi.org/10.1029/JC093iC12p15467.

Stoffelen A., Anderson D., 1997, *Scatterometer data interpretation: Estimation and validation of the transfer function CMOD4*, J. Geophys. Res., 102 (C3), 5767–5780, http://dx.doi.org/10.1029/96JC02860.

Valenzuela G. R., 1978, *Theories for the interaction of electromagnetic and oceanic waves: A review*, Bound.-Lay. Meteorol., 13, 61–85.

Zhurbas V. M., Stipa T., Mälkki P., Paka V. T., Kuz'mina N. P., Sklyarov E. V., 2004, *Mesoscale variability of the upwelling in the southeastern Baltic Sea: IR images and numerical modeling*, Oceanology, 44 (5), 619–628.

Zhurbas V., Lannemets J., Vahtera E., 2008, *Modeling of the mesoscale structure of coupled upwelling/downwelling events and the related input to the upper mixed layer in the Gulf of Finland, Baltic Sea*, J. Geophys. Res., 113, C05004, http://dx.doi.org/10.1029/2007JC004280.